Patterns of imbricate thrusting

John H. Shaw* *Department of Earth and Planetary Sciences, Harvard University, Cambridge, Massachusetts 02138*
Frank Bilotti *Texaco Exploration and Production Technology Department, Houston, Texas 77042*
Peter A. Brennan *Consultant, 5003 Plantation Colony Court, Sugar Land, Texas 77478*

ABSTRACT

Through the use of seismic reflection profiles, satellite images, and balanced kinematic models, we describe patterns that help to identify imbricate structures and define the sequence of thrusting in fold-and-thrust belts. Measures of folding shear strains are employed to define break-forward systems in which younger, deeper faults refold overlying thrust sheets. In contrast, break-backward sequences form a wide range of viable geometries that are not expected to conserve these folding strains. Thus, measures of folding shear strains provide a means to define thrusting sequence. We also explore map-view patterns of imbricate thrusting by using three-dimensional models and stereoscopic satellite images. We present an example from the Peruvian Andes in which these map patterns are combined with seismic reflection profiles to define a complex imbricate system with components of both break-forward and break-backward thrusting. These integrated methods provide new tools for understanding the deformational histories of fold-and-thrust belts, including the definition of complex structural closures with opportunities for hydrocarbon-reservoir duplication.

INTRODUCTION

Imbricate structures form by the stacking of two or more thrust sheets (Fig. 1) and are common in fold-and-thrust belts worldwide (Dahlstrom, 1969, 1970; Price, 1981; Boyer and Elliot, 1982; Suppe, 1983; McClay and Price, 1981). Imbricate structures can develop by "break-forward" propagation of thrust sheets (Suppe, 1983), by "break-backward" thrusting, or with generally coeval motion along deep and shallow faults (Boyer, 1992). We use balanced kinematic models to describe characteristic fold patterns that are used to identify imbricate structures and to distinguish among these thrusting sequences. We employ area-balance and strain-compatibility constraints, which are not limited by bed-thickness conservation, to construct kinematically viable interpretations of seismic reflection profiles and cross sections that reflect proper thrusting sequence. We also compare map patterns of three-dimensional models with surface images to identify imbricate systems and infer thrusting sequences.

IMBRICATE PATTERNS IN CROSS SECTION

Imbricate structures have complex shapes in cross section that reflect fault geometries, detachment levels, folding mechanisms, and thrusting sequence (Fig. 1). Suppe (1983) described the kinematic development of an imbricate fault-bend folding model in which both the shallow thrust fault and overlying anticline are folded above a ramp in a deeper, forward-breaking fault (Fig. 2). Parts of the older thrust sheet are refolded in kink bands generated by the deeper thrust. Thus, break-forward thrust imbrication yields fold limbs with multiple dip domains that are bounded by axial surfaces. Suppe (1983) and Mount (1989) provided equations and tabular solutions for imbricated fold-limb dips that are generated above thrust ramps stepping up from detachments. In these solutions, bed length and thickness are preserved.

We describe a new method to construct balanced interpretations for a wider range of imbricate structures, including cases without detachments and/or where bed thickness is not preserved. Our method accounts for folding shear strains—a measure of deformation caused by each thrust sheet—to predict amounts of refolding in break-forward sequences. Folding shear strains also provide a means to define thrusting sequence.

Folding shear strain is an angular measure of the change in orientation of beds and faults across a fold limb or kink band. To account for folding shear strains, we measure folding vectors that correspond to the deflection of bedding and faults across a kink band parallel to the bounding axial surface(s) (Fig. 3). In a break-forward sequence, the folding shear strain of beds in the younger kink band must be accommodated by refolding of the older, overlying thrust sheet to conserve area during deformation. Thus, the folding vector of bedding in the deep kink band must equal the amount of deflection in the overlying, folded thrust (Fig. 3B). The folding strain also is accommodated in refolded beds above the shallow thrust if cross-sectional area is conserved. Commonly, the axial-surface orientation changes above the shallow thrust, perhaps preserving layer thickness. Thus, the folding vector of the shallow fault measured along the new axial-surface orientation must equal the deflection of refolded beds in its hanging wall (Fig. 3C).

The technique of accounting for folding shear strains and folding vectors in break-forward imbricate structures is applicable to both detachment and nondetachment systems, as well as to systems containing more than two faults. This method relies on a geometric approximation of folding in thrust sheets as simple shear parallel to axial surfaces. The method can account for lateral changes in shear magnitude that may produce angular or curved fold hinges (Suppe et al., 1997). Nevertheless, the applicability of this technique will depend on the interpreter's ability to separate imbricate structures into dip domains or kink bands that share common shear (axial-surface) orientations (Mount et al., 1990; Tearpock and Bischke, 1991; Shaw et al., 1994). If axial surfaces generally bisect interlimb angles, then bed length and thickness are conserved (Suppe, 1983). Alternatively, axial surfaces may have a range of orientations that do not bisect interlimb angles where bed thickness is not conserved.

In practice, we suggest that axial-surface orientations are more readily defined from surface exposures and on seismic reflection data than are fault shapes or minor bed-thickness variations. Our method uses these easily defined axial surfaces to interpret imbricate structures (Fig. 4), while avoiding

*E-mail: shaw@eps.harvard.edu.

GSA Bulletin; August 1999; v. 111; no. 8; p. 1140–1154; 14 figures.

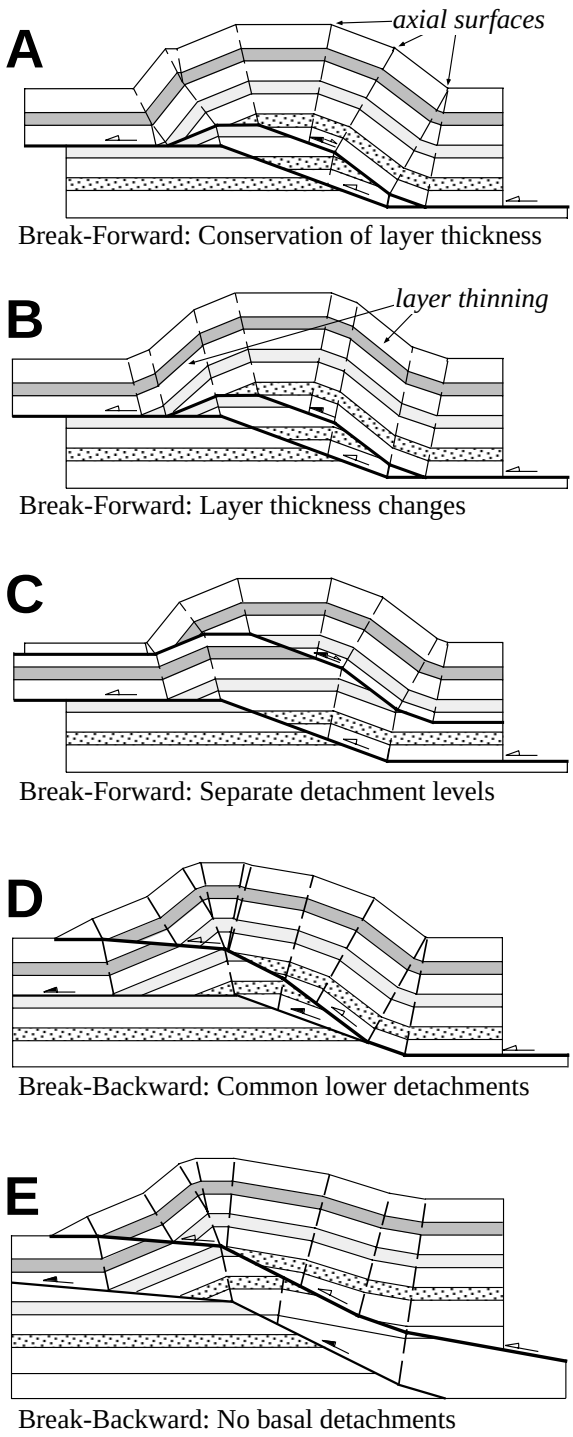

Figure 1. Balanced models of imbricate structures in which open arrows define the younger thrusts. (A) Break-forward imbricate structure with two thrusts joining at the same detachment level (Suppe, 1983). Axial surfaces bisect interlimb angles so that layer thicknesses are preserved. (B) Break-forward imbricate structure with backlimb and forelimb thinning where axial surfaces formed by the younger thrust do not bisect the interlimb angle. (C) Break-forward imbricate structure with two thrusts at separate detachment levels. (D) Break-backward imbricate structure with thrusts joining at a common basal detachment. (E) Break-backward imbricate system without basal detachments. Layer thicknesses are preserved in models C, D, and E. Slip entering and exiting all models reflects offsets on the younger thrusts, as well as slip induced on refolded thrusts to conserve layer thicknesses, where applicable.

a priori assumptions of fault geometry (for example, ramp step-up angle) or bed-thickness conservation. Thus we suggest that our approach is applicable to a wider range of imbricate geometries than previous methods, which rely on conservation of bed thickness and on bedding-parallel detachments.

Shallow thrust sheets in break-backward imbricate systems (Fig. 5) do not need to accommodate the folding shear strains of older and deeper kink bands. A fault that develops across a preexisting fold limb may have a number of viable geometries (Fig. 6). The younger, shallower fault may cut straight across the older kink band, decapitating and translating part of the older structure with fault slip (Fig. 6B). Alternatively, the shallow fault may be deflected at an axial surface of the preexisting fold, translating and refolding part of the older kink band. This deflection, however, need not equal the folding shear strains of the underlying structure (Fig. 6C); thus fault bends may occur at various angles in break-backward sequences.

The difference in permissible fault deflections between break-forward and break-backward systems provides a means to distinguish thrusting sequence. If the deflection of a fault can be measured and is found to be inconsistent with the underlying folding strains, then break-backward thrusting is the most plausible interpretation (Fig. 6C). Alternatively, if the deflection of a fault is consistent with the underlying folding shear strain, then break-forward thrusting is a permissible and straightforward interpretation (Fig. 4). This offers a valuable method to distinguish thrusting sequence. However, we often are unable to measure fault deflection directly across preexisting structure without extensive subsurface data, including depth-corrected seismic reflection profiles (Fig. 7). Nevertheless, even without these constraints, our methods of accounting for folding shear strains using folding vectors are still helpful in constructing kinematically viable cross sections where thrusting sequences are defined or implied with other data.

Other patterns of break-backward thrusts, including cases where faults break along folded bedding contacts (Fig. 6, D and E), are not always diagnostic of thrusting sequence. For example, where a shallow thrust fault is everywhere parallel to bedding, it may be impossible to distinguish a folded detachment in a break-forward system from a break-backward thrust that simply follows a bedding plane (Fig. 6D). Moreover, certain axial surfaces in fault-related folds are active (Suppe, 1983); that is, these axial surfaces are generally pinned to fault bends at depth and actively fold hanging-wall strata (Fig. 6E). Inactive axial surfaces, which also are initiated above fault bends, are translated passively in the hanging wall with progressive fault slip. Thus, where a shallow thrust offsets an inactive axial surface (Fig. 6E), it implies a component of break-backward thrusting where slip on the shallow thrust occurred after the initial formation of the kink band by slip on the deeper thrust. However, this fault-related fold configuration also is viable in systems where deep and shallow faults slip simultaneously.

In a coeval fault system similar to that shown in Figure 6E, the shallow thrust would offset the inactive axial surface A′, identical to a break-backward system. Moreover, the shallow thrust would be refolded by the underlying fault across active axial surface A, conserving folding shear strain and locally yielding a pattern of break-forward thrusting. Thus coeval fault systems may contain elements of both break-forward and break-backward imbricate structures. This possibility illustrates that individual imbricate patterns, especially those involving detachments, are useful, but not absolute, criteria for distinguishing thrusting sequence. Ideally, several observations made over the extent of a structure can be used to define thrusting sequence. In the next sec-

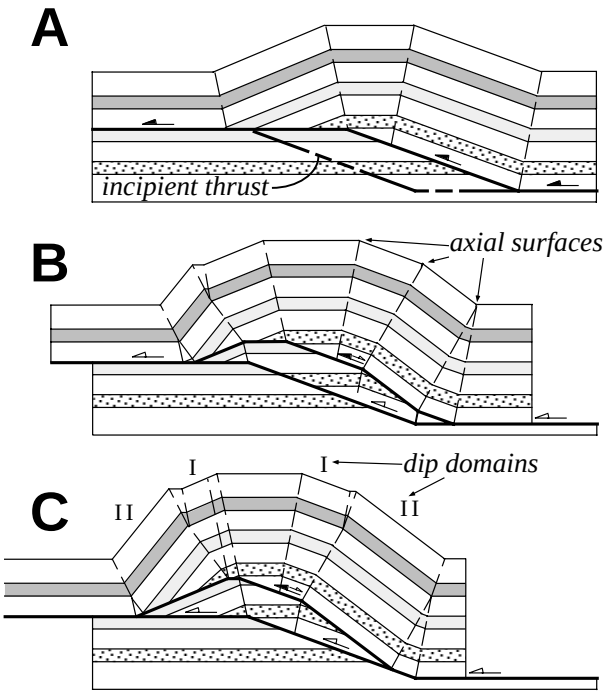

Figure 2. Sequential balanced models of a break-forward imbricate structure with thrusts sharing common detachment levels. Slip on the deep thrust refolds the overlying thrust sheet, producing fold limbs with multiple dip domains that are separated by axial surfaces (Suppe, 1983). Refolded dip domains (II) widen as fault slip increases. Layer thicknesses are preserved during refolding, causing minor reactivation of the shallow thrust.

tion, we develop this approach by exploring map-view patterns of imbricate structure that, combined with patterns in cross section, can be used to identify imbricate structures and determine thrusting sequences.

MAP PATTERNS OF IMBRICATE THRUSTING

Fold limbs with multiple dip domains that define imbricate structures in cross section (Fig. 1) also can be expressed in map view (Fig. 8). These dip domains and bounding axial surfaces are expressed on geologic maps or stereoscopic remote-sensing images by outcrop patterns and measured bedding attitudes. Moreover, measured strike and dip values can be used through fault-related folding techniques to constrain balanced subsurface interpretations (for example, Suppe, 1983; Woodward et al., 1985; De Paor, 1988; Tearpock and Bischke, 1991). However, multiple dip domains in fold limbs are not unique to imbricate thrust structures. For example, multibend fault-bend folds above a single thrust also can produce similar patterns (Medwedeff and Suppe, 1997). Thus, we explore other map-view patterns of fault-related folds to establish additional criteria for recognizing and interpreting imbricate thrust systems.

The balanced models in Figure 8 illustrate that imbricate structures have complex forms in three dimensions that are composed of multiple dip domains and arrays of axial surfaces in map view. In addition to being useful for identifying imbricate structures, these map patterns also help to define thrusting sequence. In the break-forward model of Figure 8A, a thrust ramp and hanging-wall fault-bend fold are imbricated along part of their extent

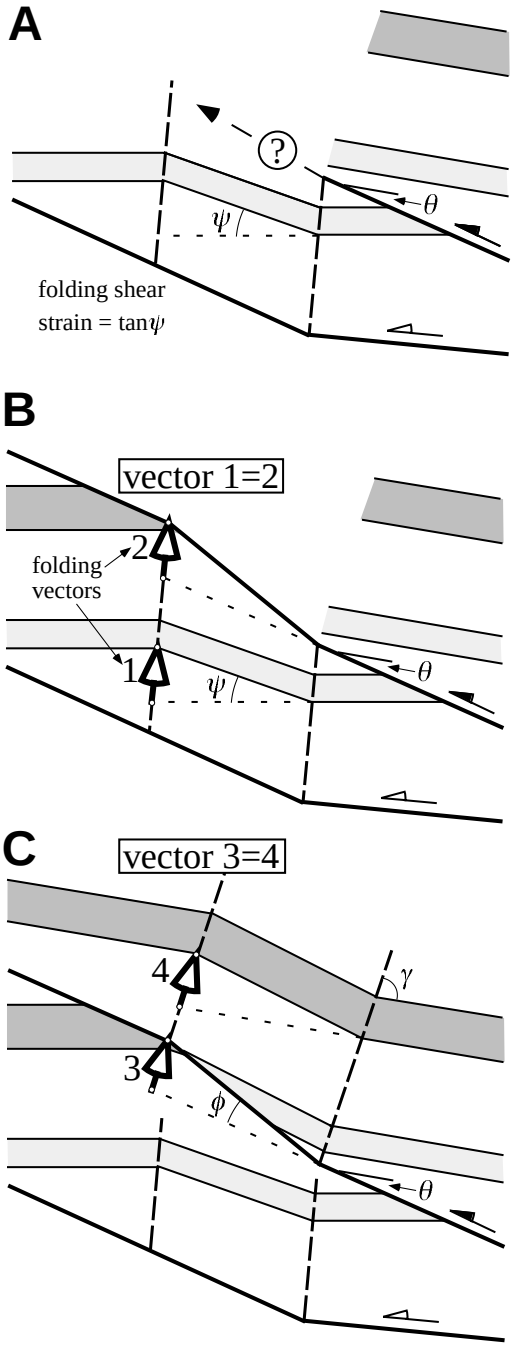

Figure 3. (A) What is the orientation of a shallow, refolded thrust across a fold limb in a break-forward imbricate system where folding shear strain (tan ψ) is accommodated? (B) Folding vector (labeled 1) in the younger and deeper kink band, which reflects folding shear strain, equals the deflection of the folded thrust (2) across the deep fold limb along the axial-surface orientation. (C) The fold shape (γ) in the shallow thrust sheet can be predicted by measuring the fault bend (ϕ) and cut-off angles (θ) through the use of fault-bend folding methods (Suppe, 1983) and the assumption that layer thicknesses are preserved. Alternatively, if the axial surfaces are readily observed in data, the deflection of the folded fault (3) should equal the folding vector (4) in the shallow thrust sheet. This latter method applies even if layer thicknesses are not preserved.

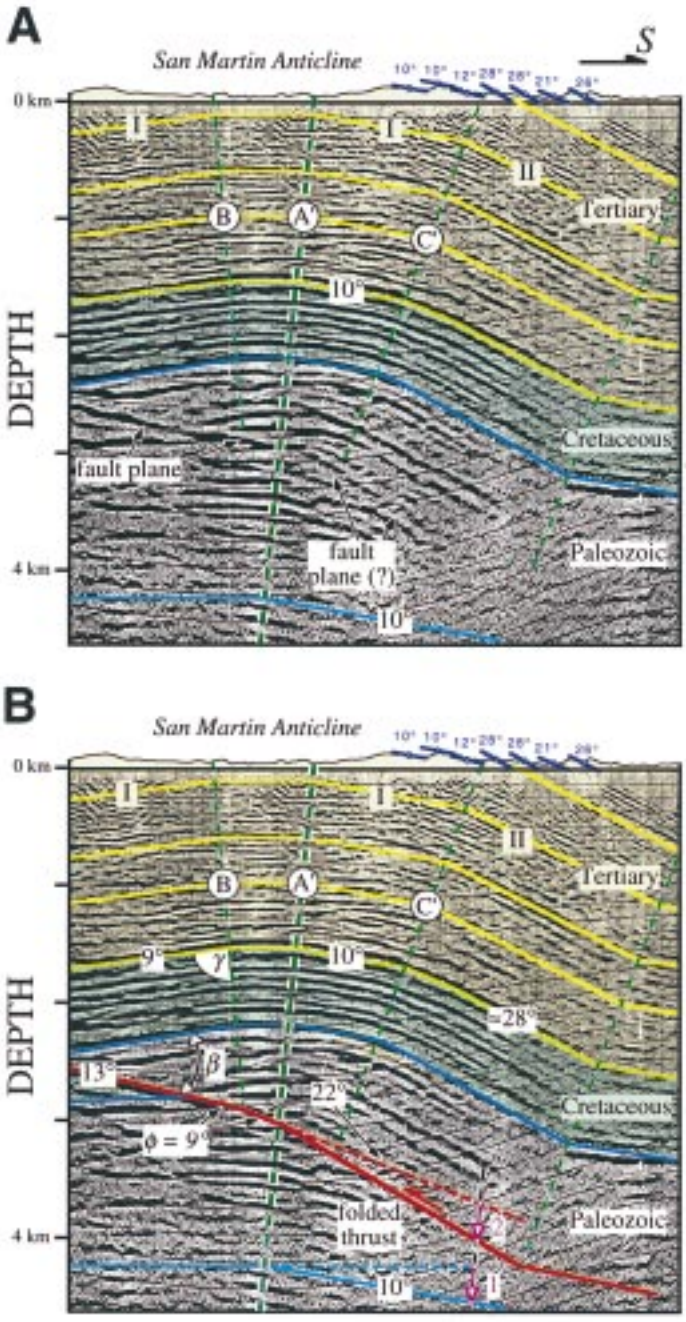

Figure 4. Migrated and depth-converted seismic reflection profile across a faulted anticline from the southern Ucayali basin, Peru. (A) Thrust fault defined by fault-plane reflection at about 2.5 km depth beneath the forelimb (left). Note that axial surface A′ extends below the observed thrust, indicating that a second, deeper fault underlies the structure. Axial surface A′ is not deflected or offset, suggesting that the shallow thrust is folded in a break-forward imbricate system. (B) Method of generating a balanced interpretation of the shallow thrust geometry in a break-forward imbricate structure. On the basis of the forelimb cut-off (β) and interlimb angle (γ) about axial surface B, the fault-bend folding theory (Suppe, 1983) predicts that the fault dip changes by 9° to a 22°S dip across axial surface B. Folding of this 22°S-dipping thrust segment across axial surface A′ by using the method of Figure 3 yields a backlimb ramp dip of about 28°S, which is roughly equal to bed dips in the refolded panel (II). The inverse folding vector (1) in the deep kink band equals the deflection of the shallow thrust (2) along the orientation of axial surface A′. Axial-surface nomenclature after Shaw et al. (1994). Seismic data provided courtesy of PERUPETRO S.A.

by a deeper thrust. Slip on the break-forward thrust (fault Y) begins between sections 1 and 2 and increases toward section 3. This slip refolds the shallow thrust sheet above fault X, producing multiple dip domains in fold limbs and additional structural relief. In map view, erosion exposes older rocks in the core of the fold (Fig. 8B). Moreover, bed contacts and axial surfaces in the shallow thrust sheet are deflected by varying amounts in the transport direction of the deep thrust. The bed contacts and anticlinal axial surfaces near the fold crest and in the forelimb are deflected most significantly. Thus, break-forward imbricate structures often have patterns of deflected axial surfaces and bed contacts that are coincident with areas of greater structural relief (Fig. 9).

In contrast to the break-forward model, the anticlinal fold axes are not translated significantly by the break-backward thrust in Figure 8C because they are linked to static elements of the subthrust structure. However, in structures where break-backward thrusts simply decapitate older structures (for example, Fig. 6B), axial surfaces may be deflected by shallow faulting, producing patterns that are somewhat similar to break-forward structures. Thus, given the wide range of possible imbricate geometries, map-view patterns of individual structures are not always fully diagnostic of thrusting sequence. However, in cases where two or more fold trends overlap along the transport direction in map view, unique fold patterns can result that help to distinguish thrusting sequences (Fig. 10).

In break-forward thrust systems, older hinterland structures are transported in the hanging walls of younger and deeper thrusts. Where slip on these younger faults varies along strike, hinterland structures commonly are deflected in the direction of thrust displacement (Fig. 10) (Snedden and Spang, 1989**;** Tearpock and Bischke, 1991). Thrusts may also be deflected in coeval fault systems or show apparent deflection due to curved faults formed as thrusts propagate toward one another, similar to common patterns of joint systems (Pollard and Aydin, 1988). In contrast, older structures in break-backward sequences do not undergo translation by deeper faults and thus are not deflected in the transport direction. Patterns of overlapping fold trends in map view, therefore, can be used to help distinguish break-forward and coeval fault systems from break-backward imbricates (Fig. 11).

AN EXAMPLE OF COMPLEX IMBRICATE THRUSTING FROM THE PERUVIAN ANDES

We conclude our discussion by presenting an analysis of several large fold trends in the Peruvian Andes that exhibit complex patterns of imbricate thrusting. The anticlinal structures (San Martin and Istmo) lie in the Andean foothills of the southern Ucayali basin (Fig. 12) and involve thrust sheets of Paleozoic through Tertiary strata (Bellido B., 1969; Mathalone and Montoya R., 1995; Geuns, 1997). Although covered by dense vegetation, the folds are directly expressed in multispectral satellite images (Fig. 12). We use these images to describe basic fold patterns as well as to derive surface bedding-attitude measurements from stereoscopic LandsatTM and SPOT imagery (Berger, 1992; Shaw et al., 1997). The stereoscopically derived measurements are combined with high-quality seismic reflection profiles (Fig. 13) to define the imbricate geometries and thrusting sequence. Notably, the surface measurements are very consistent with shallow dips imaged on depth-converted seismic reflection data (Figs. 12 and 13).

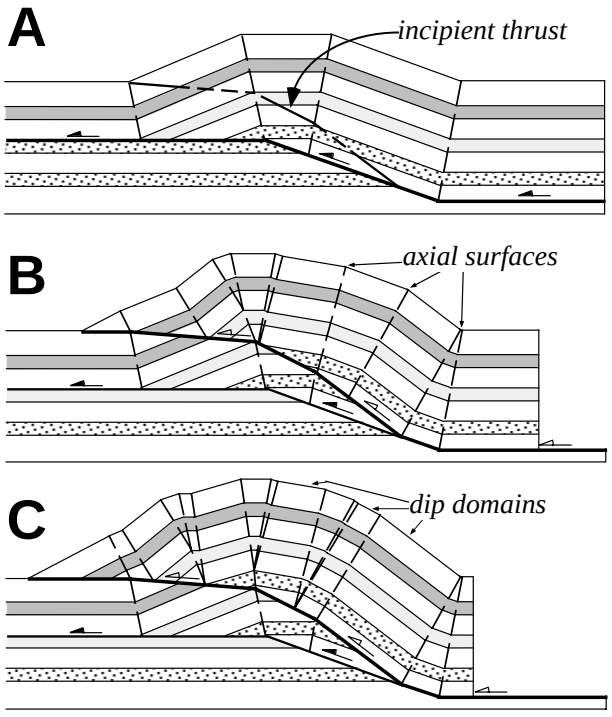

Figure 5. Sequential balanced models of a break-backward imbricate structure with thrusts joining at a common basal detachment. Slip on the break-backward thrust displaces and refolds parts of the shallow thrust sheet, producing fold limbs with multiple dip domains separated by axial surfaces. Layer thicknesses are preserved.

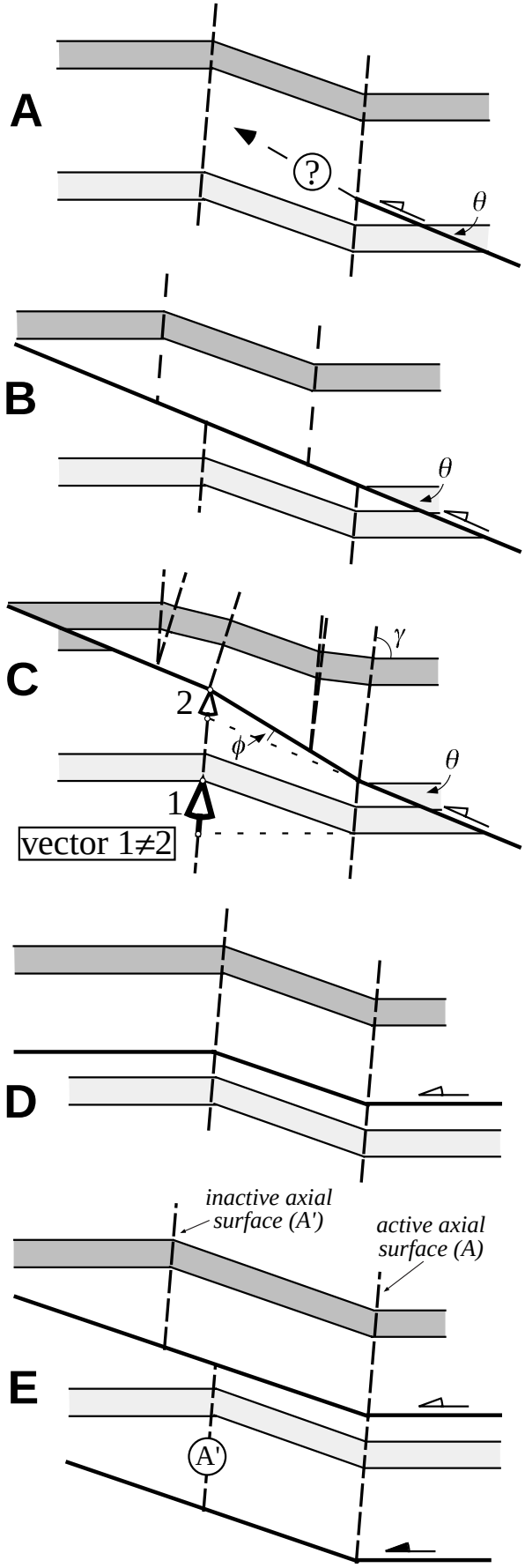

Figure 6. (A) What are possible orientations for a shallow, break-backward thrust cutting across an older fold limb? (B) The shallow thrust cuts across and offsets a part of the fold limb without changing fault orientation. (C) The shallow thrust changes its orientation across the fold limb, offsetting and refolding parts of the structure. Note that the deep folding vector (1) need not equal the deflection of the break-backward thrust (2), in contrast to the break-forward example described in Figure 3. (D) Shallow thrust following bedding planes across the fold limb. Note that this geometry also could be generated by folding a detachment in a break-forward imbricate system. (E) Shallow break-backward thrust following bedding across an active axial surface (Suppe, 1983) pinned to a deeper fault bend. The shallow thrust cuts across and offsets the inactive axial surface, which is not fixed to the underlying thrust. Both models D and E contain fault geometries that also are stable in imbricate systems with coeval deep and shallow thrusting.

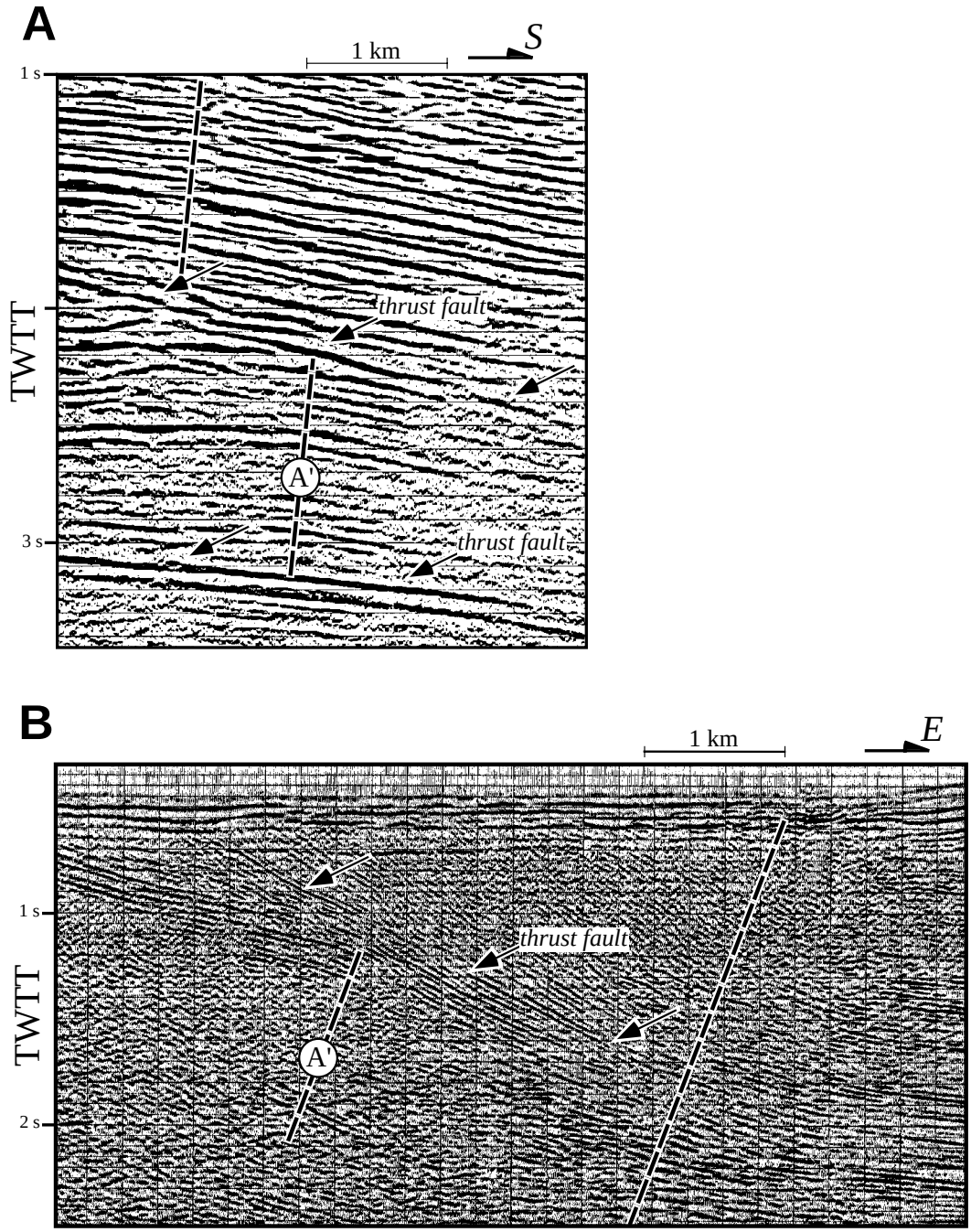

Figure 7. Migrated seismic reflection profiles across break-backward or coeval imbricate thrust systems. Note that in both cases the shallow thrust is not deflected across axial surface A′, but rather offsets the axial surface, similar to the situation in Figure 6E. (A) Seismic profile with prominent fault-plane reflections from the Ucayali basin, Peru, provided courtesy of PERUPETRO S.A. (B) Seismic profile from the Puna, Argentina, provided courtesy of Texaco. TWTT—two-way traveltime.

The San Martin anticline (Fig. 12) trends approximately east for more than 60 km and is imaged in seismic profile Y-Y′ (Fig. 13) near its eastern termination. The San Martin fold consists of a crest separating north- and south-dipping fold limbs, which are expressed at the surface as flatirons (Fig. 12) and are imaged in the seismic data (Fig. 13). Beds in the southern limb of the anticline dip most steeply near the river bed and more shallowly to the north. Thus, the southern fold limb is composed of at least two dip domains separated by axial surface C′. This geometry suggests that the San Martin structure may be imbricated above two or more thrusts. Seismic profile Y-Y′ illustrates that shallow parts of the San Martin anticline are developed above the San Martin thrust fault, which produces a prominent fault-plane reflection at about 2.5 km depth (Fig. 13). Parts of the fold extending below the San Martin thrust suggest that the structure is imbricated above a deeper fault, consistent with the two dip domains observed in the southern fold limb.

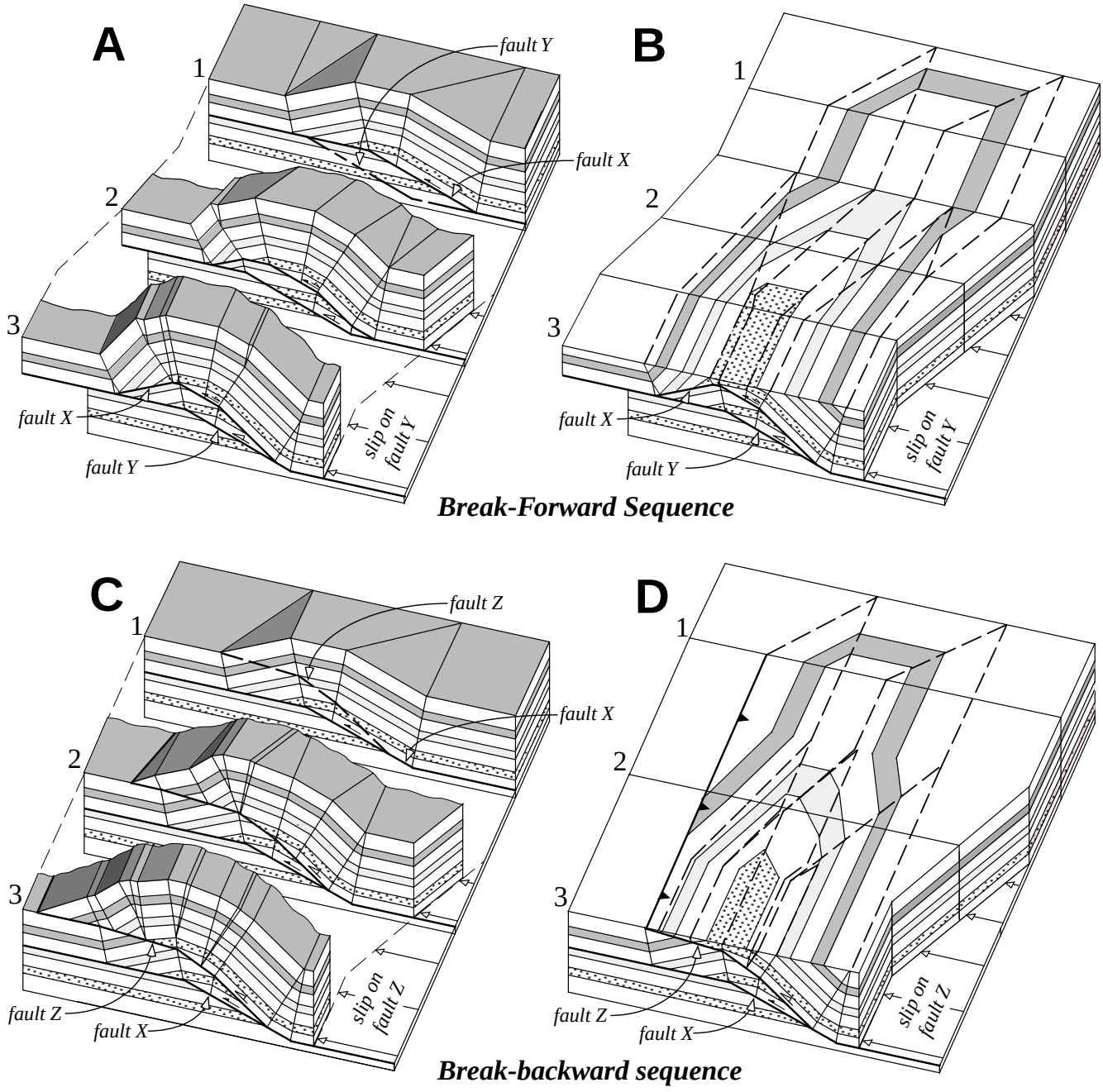

Figure 8. Perspective views of three-dimensional imbricate structures. (A) Break-forward imbricate structure with two faults (X and Y) that share common upper and lower detachments. Slip on break-forward thrust Y begins between sections 1 and 2 and increases toward section 3. (B) View of break-forward imbricate structure at a horizontal erosion level. Note the prominent map-view deflection of axial surfaces and bedding contacts caused by motion on the break-forward thrust Y. (C) Break-backward imbricate structure with two faults (X and Z) sharing a common basal detachment. Slip on break-backward thrust Z begins between sections 1 and 2 and increases toward section 3. (D) View of break-backward imbricate structure at a horizontal erosion level. Although anticlinal axial surfaces are not obviously deflected in the break-backward model, the break-backward and break-forward models share many other characteristics. These include multiple map-view dip domains and deflected bed contacts that are coincident with exposures of older strata in the fold cores.

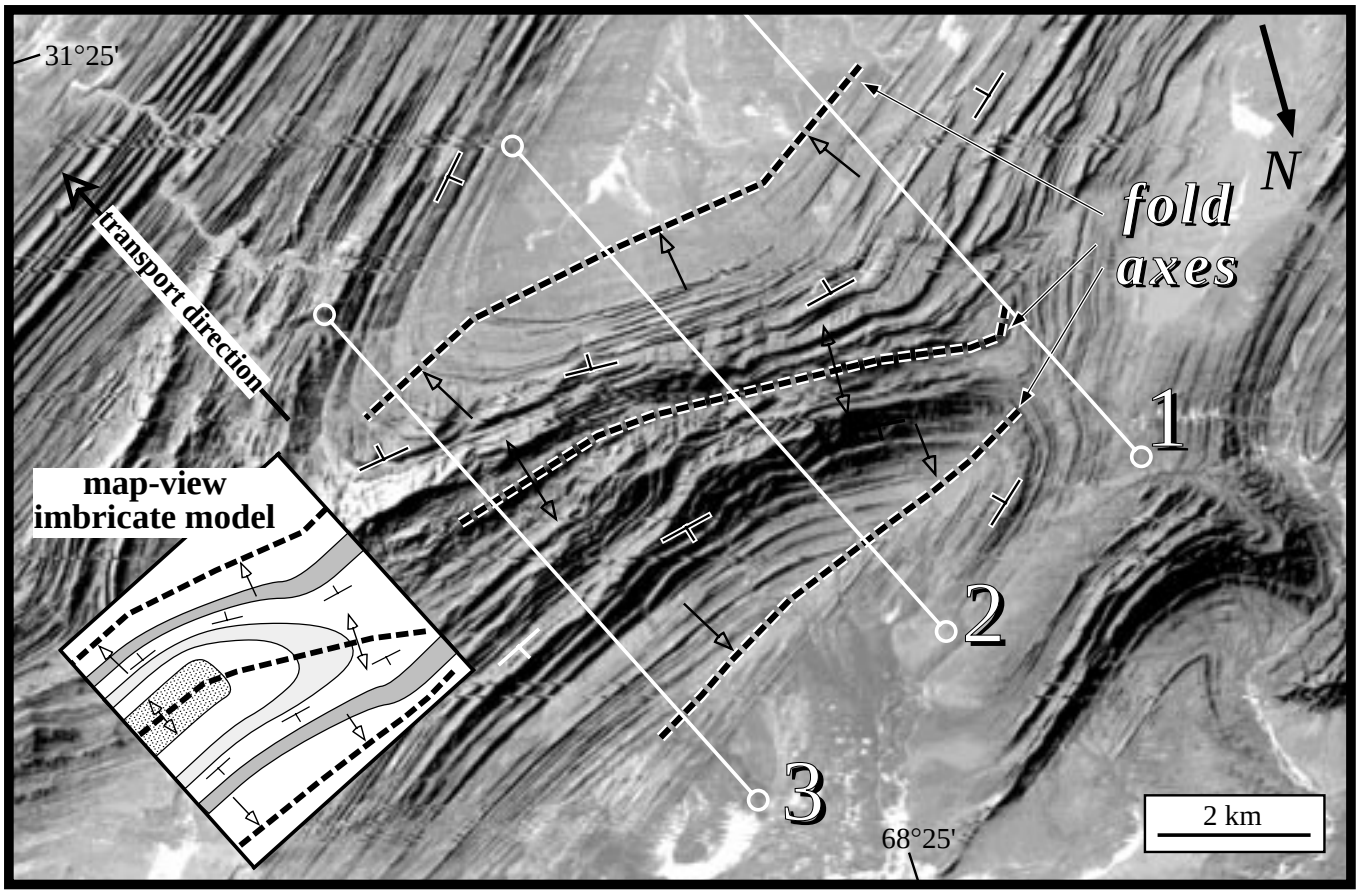

Figure 9. Landsat thematic mapper image of an anticlinal trend in the Katawaz basin, Pakistan. Deflection of the anticlinal fold axis from section 1 to section 3 corresponds with exposure of older strata in the fold core, analogous to patterns of break-forward imbricate thrusting in Figure 8B. Section traces are provided as a reference frame for comparison between the image and imbricate models (Fig. 8).

The Istmo anticline lies northeast of the San Martin structure (Fig. 12) and is developed above a second fault, the Istmo thrust, which also is imaged by a fault-plane reflection (Fig. 13). Along section Y-Y′, the south-dipping Istmo thrust extends beneath the San Martin anticline. Our projection of the Istmo thrust beneath the San Martin anticline, guided by fault-bend fold theory (Suppe, 1983), is consistent with the shape of the subthrust fold. Thus, we suggest that slip on the Istmo thrust generated this deep fold and imbricated the overlying San Martin thrust sheet.

The part of the San Martin structure that is imbricated by the Istmo thrust corresponds to the overlap of the two fold trends in map view (Fig. 12). West of the imbricated zone, the southern limb of the San Martin thrust dips uniformly between 8° and 12°S. The steeper, refolded kink band (20°–30° dip) is not present and therefore did not generate the prominent flatirons present in the imbricated zone. Thus, the map-view pattern of the southern limb of the San Martin trend, including axial surface C′ (Fig. 12), clearly defines the extent of thrust imbrication, which is corroborated by the seismic reflection data (Fig. 13). Notably, this imbricated zone coincides with a structurally high area of the San Martin fold because slip on both the San Martin and Istmo thrusts contributed to its uplift and structural relief.

Seismic profile Y-Y′ also provides insight into the thrusting sequence of the San Martin and Istmo faults. The deflection of the San Martin thrust on the south side of the San Martin anticline is consistent with the folding shear strain of the underlying kink band, as described previously with respect to Figure 4. We interpret the deep kink band to be generated above the Istmo thrust (Fig. 13). Thus, the shape of the San Martin fault is compatible with its having been refolded above the Istmo thrust in a break-forward or coeval thrust system. In contrast, the north limb of the San Martin anticline impinges on the back limb of the Istmo fold, but is not refolded by the deeper kink band (Fig. 12). If the Istmo fault had slipped after the San Martin thrust, then the forelimb of the San Martin structure should be folded above the Istmo structure, which it is not. The forelimb pattern indicates, therefore, that some of the slip on the San Martin thrust occurred after motion ceased on the Istmo fault, which is consistent with a break-backward fault system. Thus, the seismic section provides conflicting evidence about the thrusting sequence. To help resolve this ambiguity, we next explore map-view patterns of these imbricate structures.

The area where the San Martin structure is imbricated by the Istmo thrust corresponds to the zone of overlap between the anticlinal trends, as reflected in the satellite imagery (Fig. 12). In this zone, the anticlinal axis of the San Martin anticline is deflected to the north as the width, structural relief, and slip on the Istmo trend increase to the east. This anticlinal deflection is similar to the break-forward and coeval imbricate fold patterns depicted in Figures 8B and 10 and contrasts with the break-backward map-view patterns of Figure 8D. Thus, the map-view pattern is consistent with the refolding of

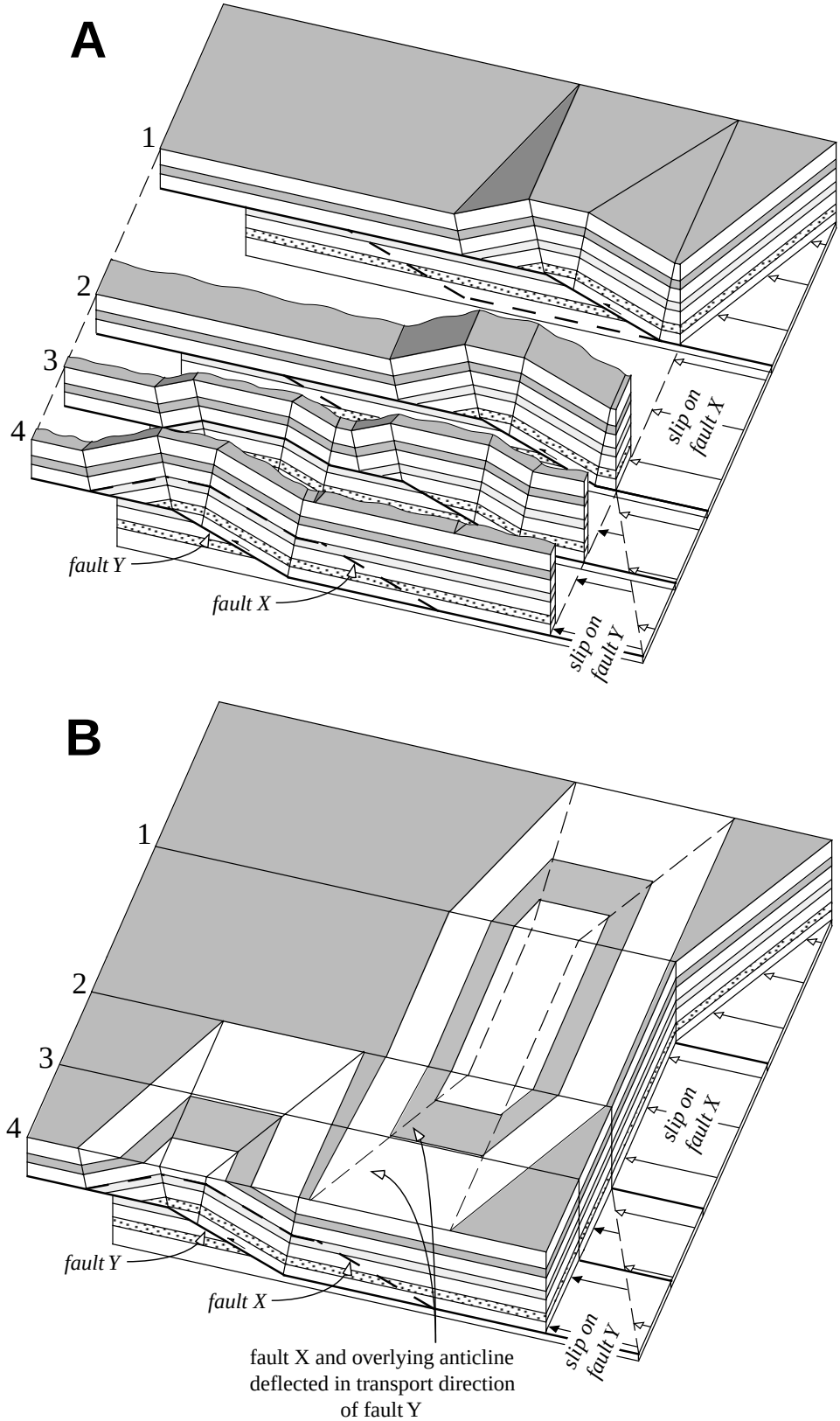

Figure 10. Perspective views of en echelon fault-bend folds developed above break-forward or coeval thrusts. (A) A fault-bend fold is developed above a ramp in fault X, on which slip decreases in both directions along strike (open arrows). Slip on frontal thrust Y begins between sections 2 and 3 and increases toward section 4. (B) View of the en echelon folds at a horizontal erosion level. Slip on fault Y transports fault X and its overlying structure, causing a map-view deflection of the fault-bend fold above ramp X in the transport direction of thrust Y. Asymmetry between the plunging noses of the fold above fault X contrasts with symmetric models of doubly plunging fault-related folds that are not affected by break-forward thrusting (Wilkerson et al., 1991).

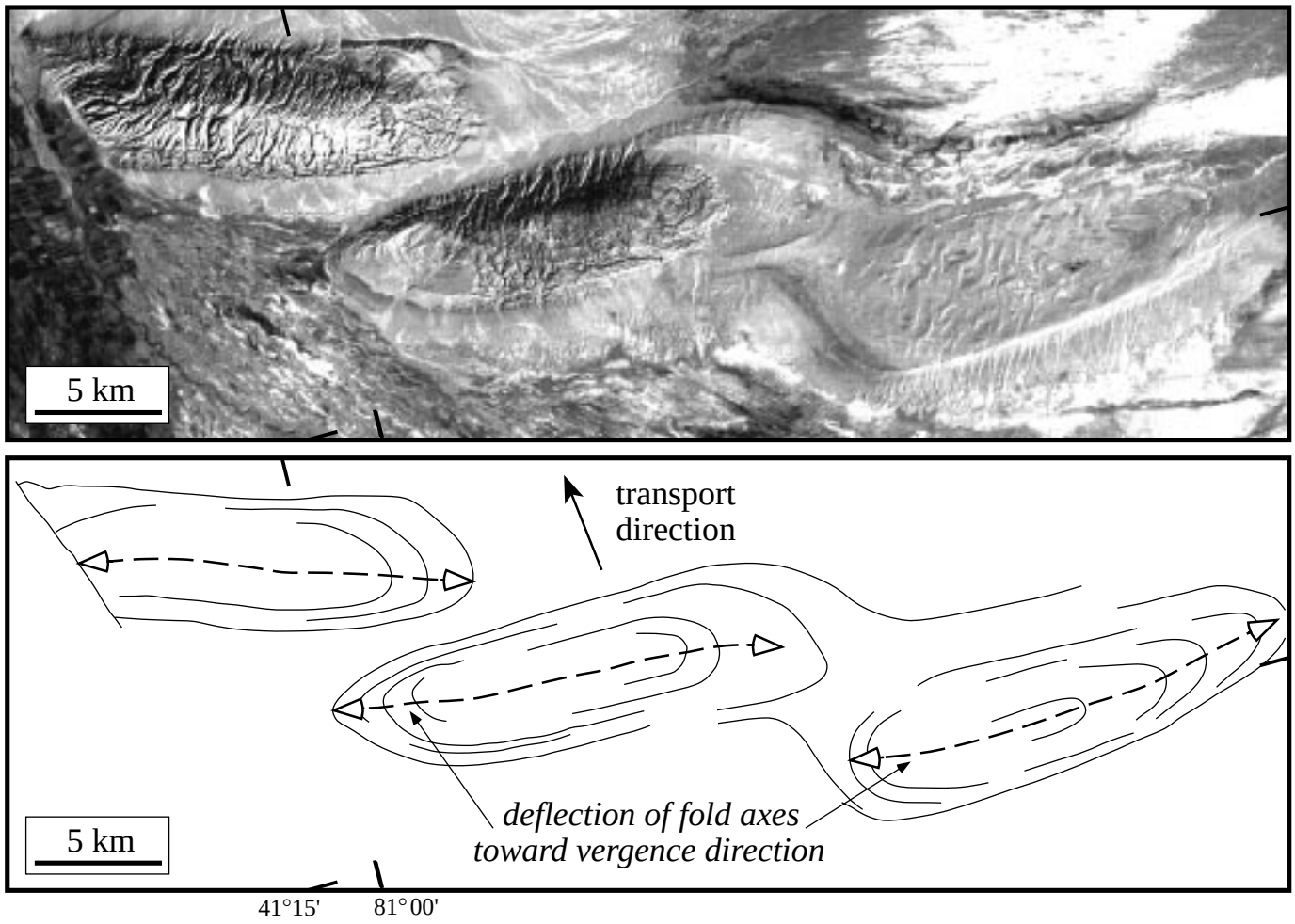

Figure 11. Landsat thematic mapper image of en echelon anticlines from the northwestern Tarim basin, China. Note the asymmetry of the anticlines, with deflection of the fold axes in the transport direction of the structures where folds overlap. This pattern is interpreted to reflect a component of break-forward thrusting, similar to the models in Figure 11. The fold asymmetry is not diagnostic of structural vergence or transport direction, which is inferred from seismic data published and interpreted by Nishidai and Berry (1990).

the San Martin thrust on the south limb of the San Martin anticline, both of which suggest break-forward or coeval thrust motion. Recall, however, that these indications are in contrast with the truncation of the southern limb of the Istmo anticline by the San Martin thrust in cross section (Fig. 13), which suggests a component of break-backward thrusting.

We propose that these conflicting fold and fault patterns result from a complex slip history on the San Martin and Istmo faults (Fig. 14). If the faults formed simultaneously, but the majority of early slip occurred on the Istmo thrust, this would cause refolding in cross section (Fig. 4) and map-view deflection (Fig. 12) of the San Martin thrust as observed. After motion on the Istmo thrust ceased, slip on the San Martin thrust (Fig. 14C) would truncate the southern limb of the Istmo anticline as imaged in the seismic profile (Fig. 13). Thus generally coeval, but episodic fault motions can produce all of the local imbricate patterns, which considered individually would yield conflicting results. This statement illustrates that recognition of several fold and fault patterns, dispersed across the structure in cross section and map view, is the most powerful approach to defining the sequence of imbricate thrusting.

SUMMARY AND CONCLUSIONS

Methods of identifying imbricate systems and defining thrusting sequence have important applications. The number, amount of slip, and relative timing of thrust faults must be determined to assess properly the magnitudes and rates of crustal shortening in fold-and-thrust belts. In tectonically active areas, imbricate structures may contain several faults that can cause damaging earthquakes. Thus, recognition and proper definition of these structures can be important for hazards assessment. Moreover, imbricate structures commonly form fold and fault closures with repetition of reservoir strata to yield large hydrocarbon traps. Thrusting sequence also can influence the thermal maturation of hydrocarbons and charge pathways for these traps, such that proper definition of imbricate structures is important for hydrocarbon exploration. Thus, we defined patterns in cross section and map view that help to identify imbricate structures and define thrusting sequences.

Measures of folding shear strain in cross section help to distinguish

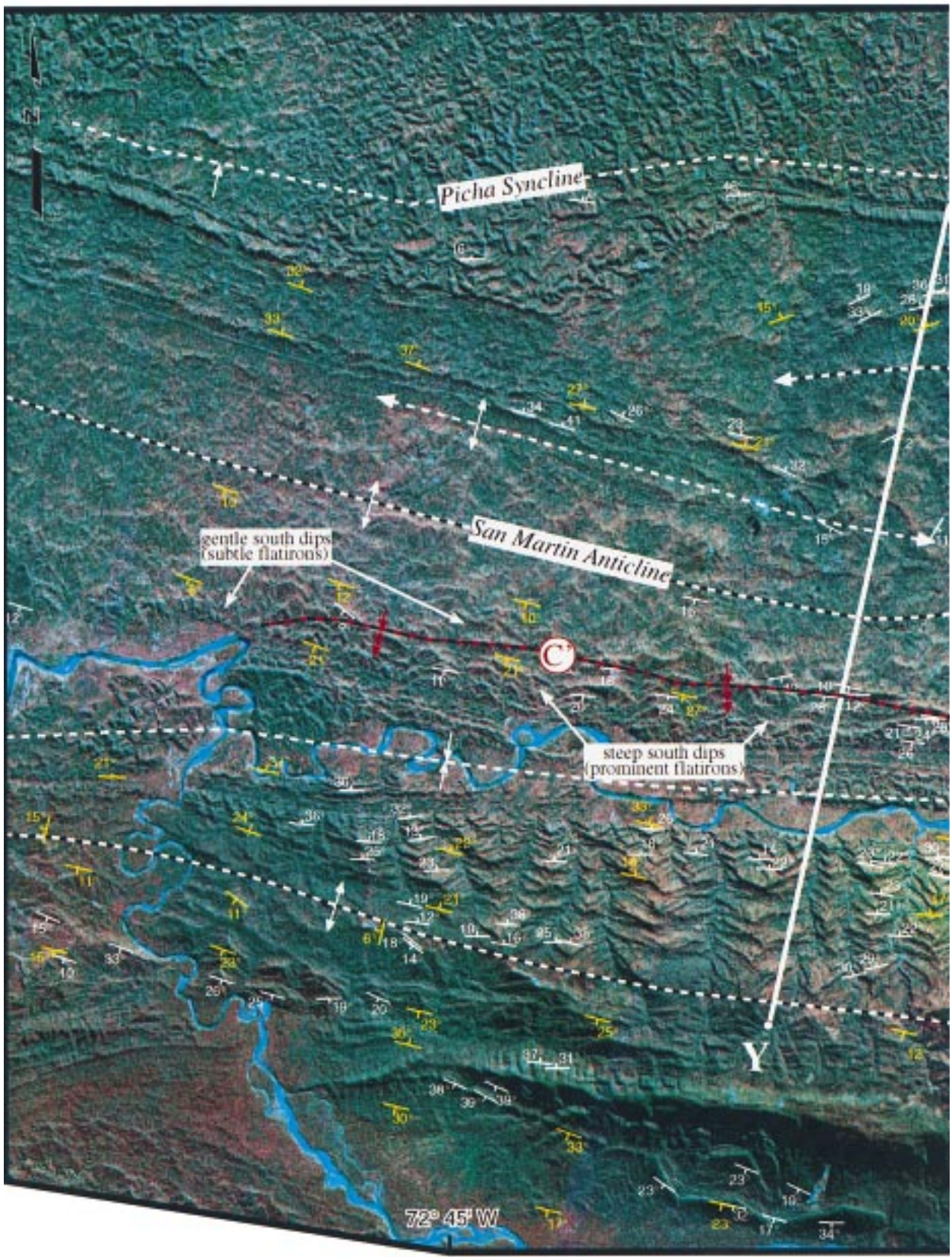

Figure 12. SPOT multispectral image of the San Martin, Istmo, and Cashiriari imbricate structures in the southern Ucayali basin, Peru. Surface attitude measurements are obtained from bedding contacts in flatirons by using stereoscopic SPOT and Landsat thematic mapper imagery. Stereoscopically derived strikes and dips generally are consistent with attitudes from shallow reflections on seismic depth profiles and are used to interpret fold patterns indicative of the imbricate thrusting and faulting sequence. The zone of en echelon overlap between the Istmo and San Martin folds corresponds to the region where the San Martin thrust is imbricated above the Istmo fault. Imbrication is expressed by multiple dip

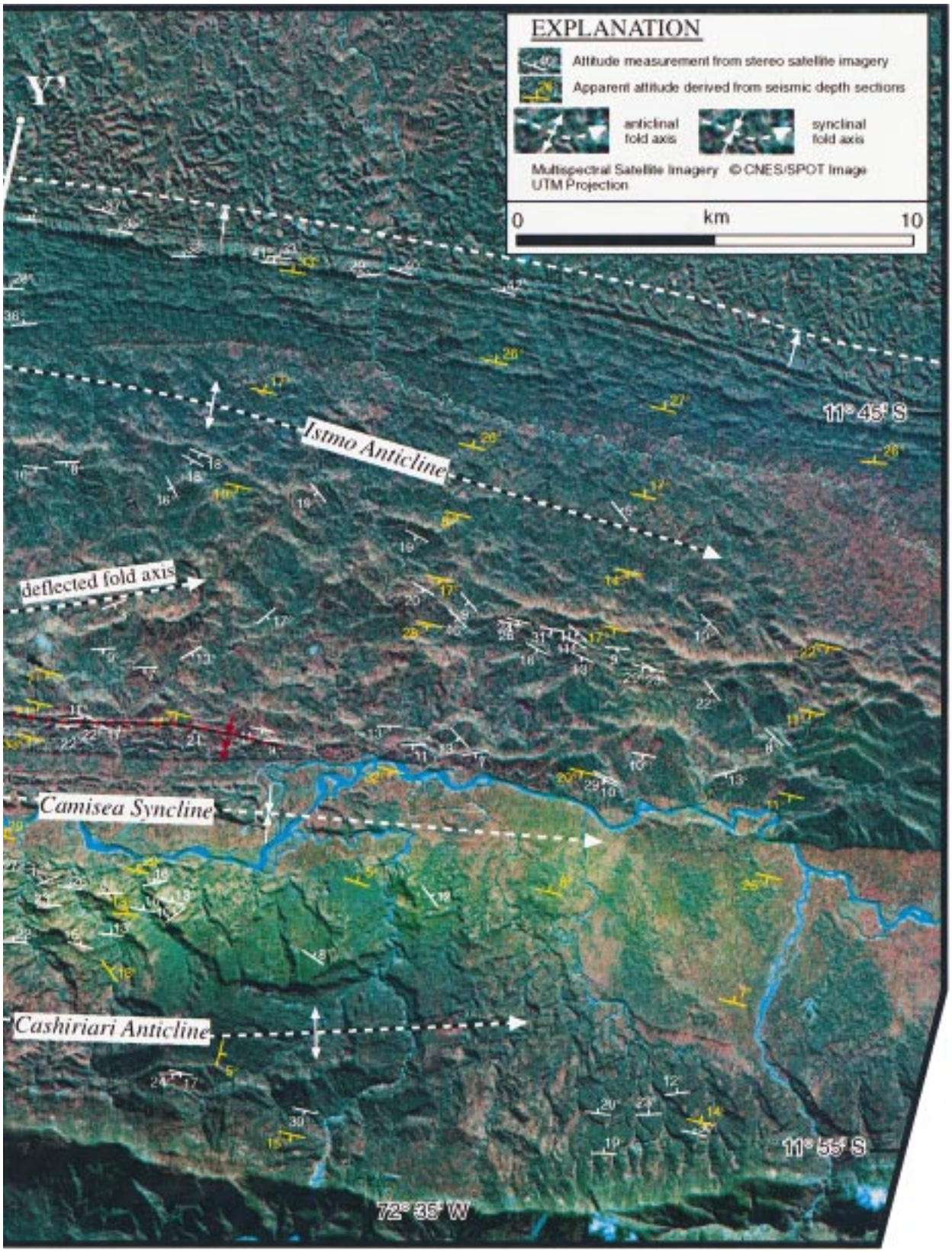

Figure 12 (*Continued*). domains that are separated by axial surface C′ on the south limb of the San Martin anticline, as well as map-view deflection of the San Martin trend toward the northward transport direction of the Istmo thrust. Line Y–Y′ is the location of the migrated seismic depth profile in Figure 13. Attitude measurements from seismic depth profiles are apparent values corrected to true strike and dip where obvious surface contacts provide bed strike. Image © CNES/SPOT Image.

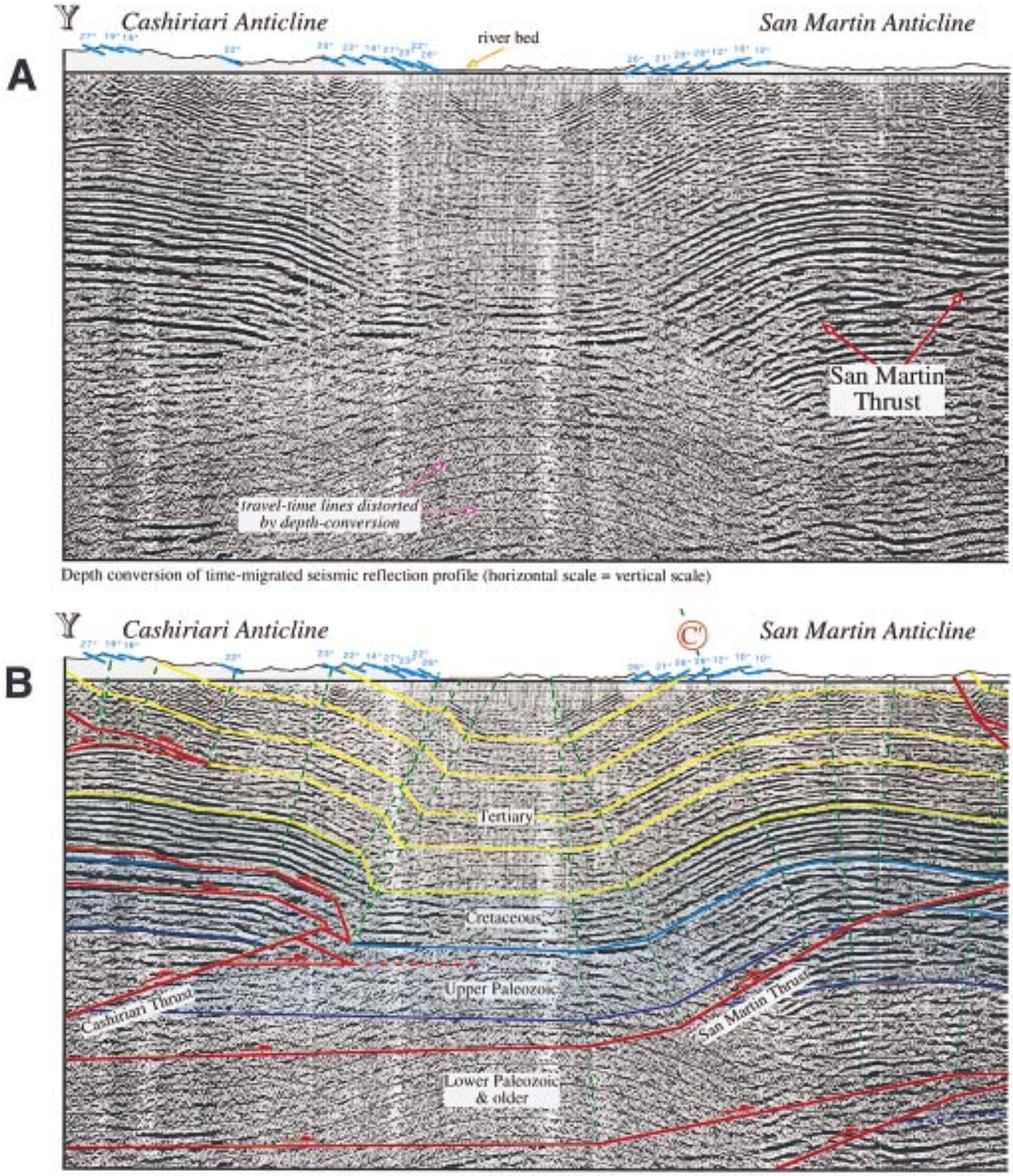

Figure 13. Time-migrated seismic reflection profile Y–Y′ converted to depth across the Cashiriari, San Martin, and Istmo structures. (A) Uninterpreted section showing prominent fault-plane reflections of the San Martin and Istmo thrusts. Note the consistency between surface dips derived from the stereoscopic remote-sensing imagery and shallow reflections. (B) Interpreted profile. Multiple dip domains in the southern limb of the San Martin anticline separated by axial surface C′ are consistent with imbrication of the structure above the San Martin and Istmo thrusts. Note the upward termination of the syncline at the San Martin thrust on the south limb of the Istmo trend, indicating a component of break-backward faulting (see text for discussion). Seismic data provided courtesy of PERUPETRO S.A.

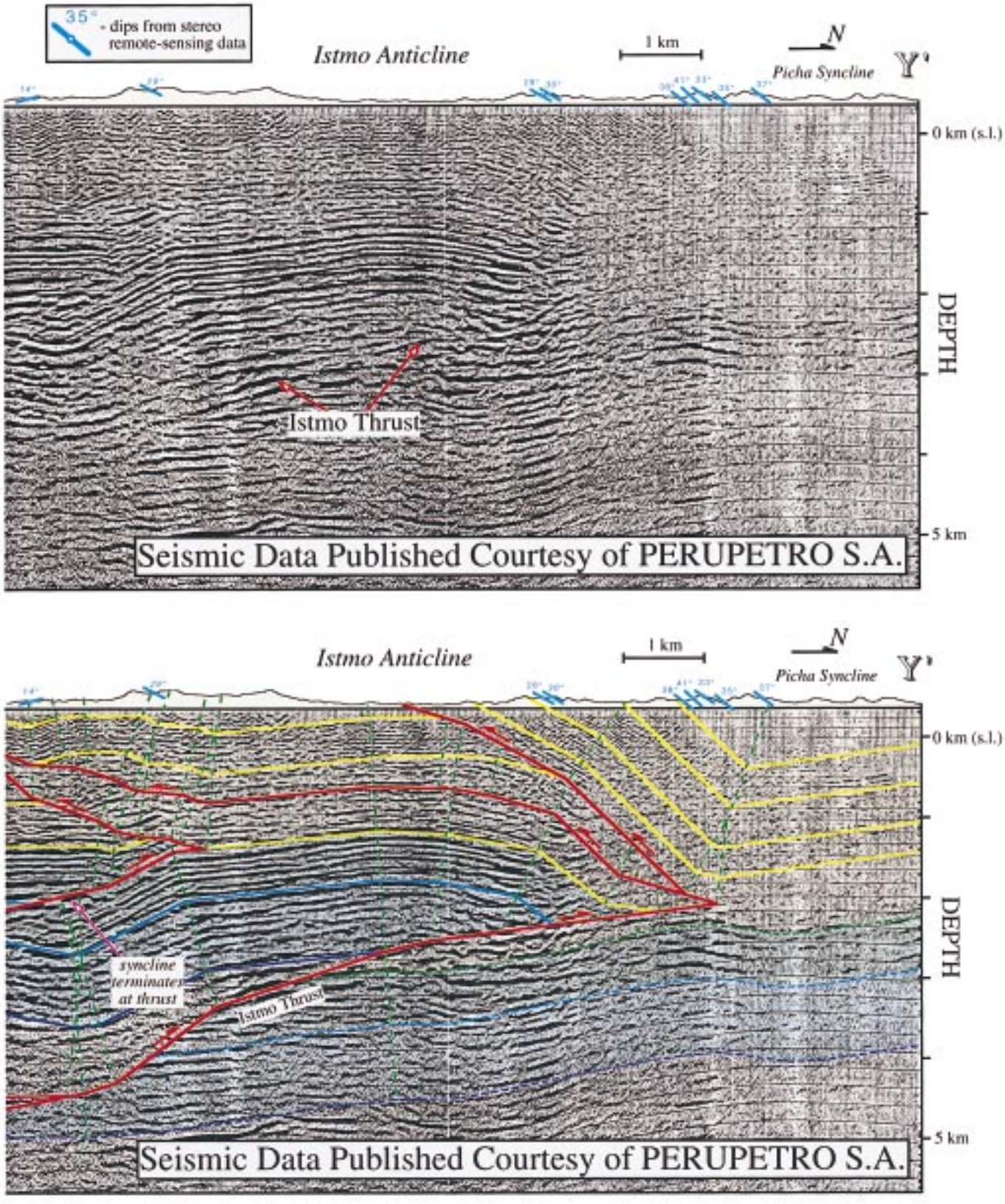

Figure 13. (*Continued*).

break-forward systems in which young faults refold overlying thrust sheets. In contrast, break-backward sequences form a wide range of viable geometries that are not expected to accommodate folding strains. In map view, multiple dip domains in fold limbs and deflected fold axes may reflect structural imbrication. However, thrusting sequence is defined best through a combination of patterns in map view and cross section. We suggest that these methods of recognizing and interpreting patterns of imbricate thrusting can be employed to understand the deformational histories of fold-and-thrust belts, as well as to define complex structural closures with opportunities for petroleum-reservoir duplication.

ACKNOWLEDGMENTS

We thank PERUPETRO S.A. and Texaco, Inc., for providing seismic reflection profiles, as well as SPOT IMAGE Corporation for permissions to publish their imagery. Landsat data used in this paper were purchased from the U.S. Geological Survey, EROS Data Center, Sioux Falls, South Dakota. Kristi Keller and Steve McDougall inspired us to work on the examples from Peru. Chris Connors provided the example from the Puna, Argentina, and along with Alfredo Prelat, Jack Carnes, Paul Genovese, and Stephen Hook gave support and guidance throughout the project. We thank M. Scott Wilkerson and Peter Vrolijk for helpful reviews.

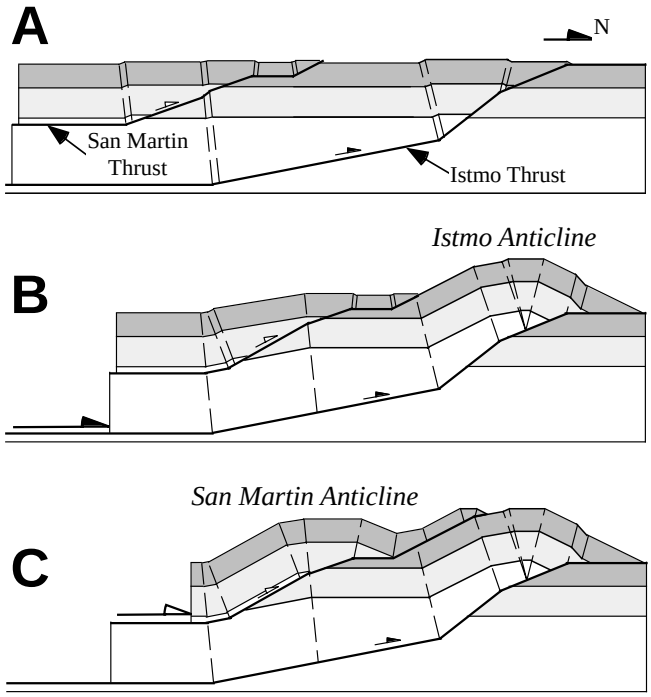

Figure 14. Balanced sequential model of the development of the San Martin and Istmo structures. A: Faults form simultaneously with minor displacement. B: Slip on the Istmo thrust forms the Istmo anticline, translating and folding the San Martin thrust sheet. C: Slip on the San Martin thrust forms the San Martin anticline, which impinges on the south limb of the Istmo fold. This simplified model depicts only pre-Tertiary strata.

REFERENCES CITED

Bellido B., E., 1969, Sinopsis de la geología del Perú: Servicio de Geología y Minería Boletín 22, 54 p.

Berger, Z., Lee Williams, T. H., and Anderson, D. W., 1992, Geologic stereo mapping of geologic structures with SPOT satellite data: American Association of Petroleum Geologists Bulletin, v. 76, p. 101–120.

Boyer, S. E., 1992, Geometric evidence for synchronous thrusting in the southern Alberta and northwest Montana thrust belts, *in* McClay, K. R., ed., Thrust tectonics: London, Chapman Hall, p. 377–390.

Boyer, S. E., and Elliot, D., 1982, Thrust systems: American Association of Petroleum Geologists Bulletin, v. 66, p. 1196–1230.

Dahlstrom, C. D. A., 1969, Balanced cross sections: Canadian Journal of Earth Sciences, v. 6, p. 743–757.

Dahlstrom, C. D. A., 1970, Structural geology in the eastern margin of Canadian Rocky Mountains: Canadian Petroleum Geology Bulletin, v. 18, p. 332–406.

De Paor, D. G., 1988, Balanced section in thrust belts: Part 1. Construction: American Association of Petroleum Geologists Bulletin, v. 72, p. 73–90.

Geuns, L. C. van, 1997, Camisea field, Peru: Revisited [abs.], *in* Oil and gas exploration and production in fold and thrust belts: American Association of Petroleum Geologists Hedberg Research Conference Proceedings, Veracruz, Mexico.

Mathalone, J. M. P., and Montoya, R. M., 1995, Petroleum geology of sub-Andean basins of Peru, *in* Tankard, A., Soruco, R. S., and Welsink, eds., Petroleum basins of South America: American Association of Petroleum Geologists Memoir 62, p. 423–444.

McClay, K. R., and Price, N. J., eds., 1981, Thrust and nappe tectonics: Geological Society [London] Special Publication 9, 544 p.

Medwedeff, D. A., and Suppe, J., 1997, Multibend fault-bend folding: Journal of Structural Geology, v. 19, p. 279–292.

Mount, V. S., 1989, State of stress in California and a seismic structural analysis of the Perdido fold belt, northwest Gulf of Mexico [Ph.D. thesis]: Princeton, New Jersey, Princeton University, 220 p.

Mount, V. S., Suppe, J., and Hook, S. C., 1990, A forward modeling strategy for balanced cross sections: American Association of Petroleum Geologists Bulletin, v. 74, p. 521–531.

Nishidai, T., and Berry, J. L., 1990, Structure and hydrocarbon potential of the Tarim Basin (NW China) from satellite imagery: Journal of Petroleum Geology, v. 13, p. 35–58.

Pollard, D. D., and Aydin, A., 1988, Progress in understanding jointing: Geological Society of America Bulletin, v. 100, p. 1181–1204.

Price, R. A., 1981, The Cordilleran foreland thrust and fold belt in the southern Canadian Rocky Mountains, *in* McClay, K. R., and Price, N. J., eds., Thrust and nappe tectonics: Geological Society [London] Special Publication 9, p. 427–448.

Shaw, J. H., Hook, S. C., and Suppe, J., 1994, Structural trend analysis by axial surface mapping: American Association of Petroleum Geologists Bulletin, v. 78, p. 700–721.

Shaw, J. H., Bilotti, F., Brennan, P. A., Connors, C. D., and Prelat, A. E., 1997, Patterns of thrust fault imbrication, en-echelon interference, and displacement transfer inferred from remote-sensing images [abs.], *in* Oil and gas exploration and production in fold and thrust belts: American Association of Petroleum Geologists Hedberg Research Conference Proceedings, Veracruz, Mexico.

Snedden, W. T., and Spang, J. H., 1989, Geometric analysis of displacement transfer between thrust faults using fault-bend and fault-propagation fold models: Geological Society of America Abstracts with Programs, v. 21, no. 6, p. A67.

Suppe, J., 1983, Geometry and kinematics of fault-bend folding: American Journal of Science, v. 283, p. 684–721.

Suppe, J., Sabat, F., Muñoz, J. A., Poblet, J., Roca, E., and Verges, J., 1997, Bed-by-bed fold growth by kink-band migration: Sant Lorenc de Morunys, eastern Pyrenees: Journal of Structural Geology, v. 19, p. 443–462.

Tearpock, D., and Bischke, R. E., 1991, Applied subsurface geological mapping: Englewood Cliffs, New Jersey, Prentice-Hall, 648 p.

Wilkerson, M. S., Medwedeff, D. A., and Marshak, S., 1991, Geometrical modeling of fault-related folds: A pseudo–three-dimensional approach: Journal of Structural Geology, v. 13, p. 801–812.

Woodward, N. B., Boyer, S. E., and Suppe, J., 1985, An outline of balanced cross-sections: University of Tennessee, Department of Geological Sciences, Studies in Geology (second edition), v. 11, 170 p.

MANUSCRIPT RECEIVED BY THE SOCIETY AUGUST 12, 1997
REVISED MANUSCRIPT RECEIVED SEPTEMBER 21, 1998
MANUSCRIPT ACCEPTED OCTOBER 6, 1998

Printed in U.S.A.